Published version available:

F. Vismarra et al., “Dynamic Interference of Chirped Photoelectrons”

Phys. Rev. Lett. **135**, 033202 – **Published 15 July, 2025**

DOI: https://doi.org/10.1103/73tl-w87y

Dynamic interference of chirped photoelectrons

Federico Vismarra,[1,2,*] Mattias Bertolino,[3,†] Elisa Appi,[3] Marius Plach,[3] Lénárd Gulyás Oldal,[4] Tímea Grósz,[4] Gian Luca Dolso,[1] Vénus Poulain,[3] Daniele Mocci,[1] Giacomo Inzani,[1] Chinmoy Biswas,[4] Massimo De Marco,[4] Gabriele Zeni,[5,6] Fabio Frassetto,[5] Luca Poletto,[5] Maurizio Reduzzi,[1] Rocio Borrego-Varillas,[2] Hans Jakob Wörner,[7] Zoltán Filus,[4] Imre Seres,[4] Péter Jójárt,[4] Balázs Major,[4] Tamás Csizmadia,[4] Mauro Nisoli,[1,2] Per Eng-Johnsson,[3,‡] Jan Marcus Dahlström,[3,§] and Matteo Lucchini[1,2,¶]

[1] *Department of Physics, Politecnico di Milano, Piazza Leonardo Da Vinci, 32, Milano, 20133, Italy*
[2] *Institute of Photonics and Nanotechnologies, IFN-CNR, Piazza Leonardo Da Vinci, 32, Milano, 20133, Italy*[†]
[3] *Department of Physics, Lund University, Box 118, Lund, 22100, Sweden*
[4] *ELI ALPS, ELI-HU Non-Profit Ltd. Wolfgang Sandner utca 3, Szeged, 6728, Hungary*
[5] *Institute of Photonics and Nanotechnologies, IFN-CNR, Padova, 35131, Italy*
[6] *CISAS - Center of Studies and Activities for Space, Via Trasea 7, Padova, 35131, Italy*
[7] *Department of Chemistry, Laboratorium für Physikalische Chemie, ETH Zürich, Vladimir-Prelog-Weg 2, Zürich, 8093, Switzerland*

(Dated: June 10, 2025)

Dynamic interference (DI) is an elusive strong-field effect where photoelectrons from intense laser pulses interfere in time, forming rich kinetic energy patterns. Here, we present the first experimental demonstration of isolated DI using a novel two-color scheme—chirped laser-assisted dynamic interference (cLADI). Isolation was achieved with a crossed-polarization setup combining an extreme ultraviolet harmonic field and an infrared pulse with tailored spectro-temporal properties. Beyond prior works, our approach enables precise control over interfering trajectories, yielding holographic interference patterns and advancing our understanding of strong-field phenomena.

Attosecond science [1, 2] has revolutionized our understanding of photoemission, demonstrating that two-color schemes and time-resolved interferometric techniques [3–5] can reveal details hidden in the phase of the outgoing electrons [6–8]. In the photoelectric effect, a photon of energy Ω_0 (atomic units are used through this work) liberates an electron from an atom with ionization potential I_p, giving it a kinetic energy $\varepsilon = \Omega_0 - I_p$. Recent theoretical works suggest that timing information from the photoemission process can be directly imprinted on the photoelectron spectrum via dynamic interference (DI) [9–11]. While an intense low-frequency ($\Omega_0 \ll I_p$) laser pulse increases the effective ionization energy by the ponderomotive potential $I_p^{\text{eff}}(t) \approx I_p + U_p(t)$ [12, 13], superintense high-frequency ($\Omega_0 > I_p$) laser pulses instead decrease the effective binding potential, $I_p^{\text{eff}}(t) \leq I_p$ [14]. In both cases, electrons emitted at different times (during the pulse rising and falling edges) may interfere to produce characteristic energy patterns.

Achieving DI requires a delicate balance: the laser field must be strong enough to induce a significant energy shift, while not completely depleting the atomic population [10, 11]. Although the original prediction of DI [9] has been dismissed (see Ref. [11]), its general idea has attracted much further theoretical attention. DI is possible only in the elusive superintense stabilization regime ($\sim 10^{18}\,\text{W/cm}^2$ at $\Omega_0 \sim 50\,\text{eV}$) for the hydrogen ground state ($1s$) [11], in intense near-resonant fields (10^{15} W/cm^2 at 12 eV) from the hydrogen excited state ($2p$) [10], and in near-resonant multiphoton processes of alkali atoms [15]. However, DI in resonant photoionization processes, where two atomic states are strongly coupled [16, 17], has been disputed [18, 19] and instead attributed to the manifestation of Rabi dynamics [20–22] – in a coherent photoelectron phenomenon predicted by Rogus and Lewenstein in 1986 [23].

More recently, M. Bertolino et al. [24] proposed that laser-assisted dynamic interference (LADI) could relax the stringent laser requirements of DI. In this two-color approach, a weak extreme-ultraviolet (XUV) pulse of central photon energy Ω_0 ionizes the sample while an intense infrared (IR) pulse of central photon energy $\omega \ll I_p < \Omega_0$ dynamically increases the binding potential. Despite its promise, unambiguous experimental observation of LADI has remained challenging mainly due to competing multiphoton (MP) processes obscuring the LADI signature [25]. In this Letter, we introduce a new regime — chirped laser-assisted dynamic interference (cLADI) — achieved with chirped XUV pulses. Our combined experimental and theoretical study demonstrates that cLADI enables robust detection of isolated DI at moderate IR intensities ($\sim 2\,\text{TW/cm}^2$) under standard laboratory conditions. Moreover, controlling the chirp of the XUV pulses adds an extra degree of freedom, allowing us to tune the number of the interfering quantum trajectories, providing new avenues in ultrafast spectroscopy [2] and deepen our understanding of fundamental light–matter interactions.

If the XUV central energy Ω_0 is high enough, the two-color photoelectron spectrum in a LADI scheme can be described within the strong-field approximation (SFA) [26–28] as the Fourier transform of the electron

wavepacket, whose phase is modulated by the IR field [29] (see Supplementary Sec. S2.1). Within the slowly-varying envelope approximation (SVEA), and for a flat continuum, the total phase term can be written as:

$$\phi(t) = \Theta(t) - (\varepsilon + I_p)\, t - \int_{-\infty}^{t} \left[\mathbf{p} \cdot \mathbf{A}_\omega(t') + \frac{A_\omega^2(t')}{2} \right] dt', \tag{1}$$

where $\Theta(t)$ is the temporal phase of the XUV field, $\mathbf{p}$ is the final electron momentum in the continuum ($\varepsilon = p^2/2$), $\mathbf{A}_\omega$ is the IR vector potential. The term $\mathbf{p} \cdot \mathbf{A}_\omega$ describes MP absorption processes responsible for the creation of sidebands separated by ω [30, 31]. If one considers only electrons emitted perpendicularly to the IR field, this term vanishes and the main contribution to the photoelectron spectrum is given by the time instants t_i for which $d\phi/dt = 0$ (stationary-phase approximation, SPA) [32]. For a given final electron energy, ε, the cycle-averaged condition is satisfied when:

$$\varepsilon(t_i) = \frac{d\Theta}{dt}(t_i) - I_p - U_p(t_i), \tag{2}$$

where and U_p is the IR ponderomotive energy, related to the field amplitude $E_{\omega,0}$ by $U_p(t) = E_{\omega,0}^2(t)/4\omega^2$. If the XUV pulse is shorter than the IR pulse, $U_p(t_i) \simeq U_{p,0}$, resulting in a redshift of the photoelectron spectrum by the peak ponderomotive energy. In contrast, for an XUV pulse longer than the IR [e.g., as in Fig. 1(a)], Eq. (2) shows that U_p dynamically changes the kinetic energy of the photoelectron during ionization, inducing an interference pattern that cannot be explained by inter- and intra-cycle mechanisms [33–35].

For a transform-limited (TL) XUV pulse with a linear phase, $\Theta(t) = \Omega_0 t$, the energy content remains constant throughout its duration [Fig. 1(b)]. In this case, $\varepsilon(t)$ follows the IR pulse intensity envelope $E_{\omega,0}^2(t)$ [Fig. 1(c)], spanning an energy range equal to $U_{p,0}$. Within this range, two families of XUV ionization events, occurring at the rising (green) and falling (orange) edges of the IR pulse, satisfy Eq. (2). Since these trajectories lead to the same final electron energy, they interfere, giving rise to a LADI pattern in the photoelectron spectrum (blue curve, right panel).

For a chirped XUV pulse with a quadratic phase $\Theta(t) = \Omega_0 t + c_\Omega t^2$ and chirp rate c_Ω, the energy content changes linearly over time [Fig. 1(d)]. $\varepsilon(t)$ exhibits an additional linear term [Fig. 1(e)], resulting in a third family of stationary solutions (chirp solutions, red markers) that contribute to the interference, modifying both the energy region with stationary solutions, $\Delta\varepsilon$, and the pattern observed in the photoelectron spectrum (blue curve in the right panel).

Figure 2 compares the IR-intensity dependence of the photoelectron spectra generated in Ne for TL [Fig. 2(a)] and chirped [Fig. 2(b)] XUV pulses, computed using the SFA formula [Figs. 2(c)-(d)] and the SPA approach

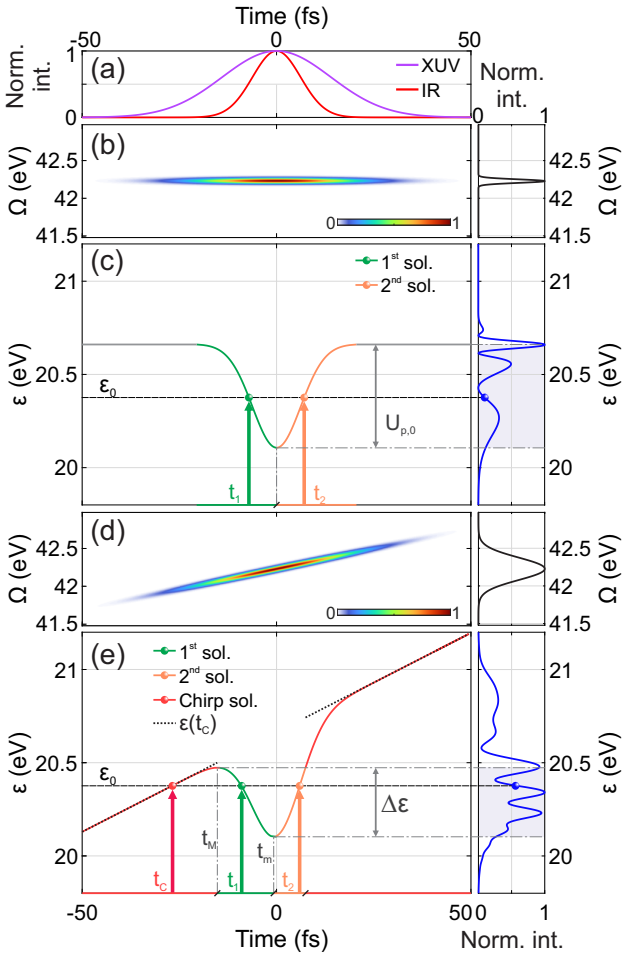

FIG. 1. **(a)** XUV (violet) and IR (red) intensity temporal profiles, corresponding to a full-width half-maximum (FWHM) duration of 32.9 fs and $\sim$ 15 fs, respectively. The IR pulse is centered around 1.166 eV while $\Omega_0 = 42.23$ eV. **(b)** Wigner transform for a transform-limited (TL) XUV pulse with temporal profile as in (a) and power spectrum displayed in the right panel (black curve). **(c)** Energy shift $\varepsilon(t)$ felt by the electron wavepacket for an IR intensity $I_{IR} \simeq 5\,\mathrm{TW/cm^2}$, when Ne is ionized by the XUV pulse in (b). IR and XUV have crossed polarization. For each final energy ε_0, two possible paths (highlighted in green and orange colors) give rise to an interference pattern in the photoelectron spectrum (blue curve, right panel). **(d)**, **(e)**, Same as in (c) and (d) but for a chirped XUV pulse with group-delay-dispersion (GDD) equal to -60 fs^2 ($c_\Omega = 8.1 \times 10^{-3}\,\mathrm{fs}^{-2}$) and a TL duration of 5.2 fs [actual FWHM duration of about 33 fs as in (a)]. In this case a third family of stationary solution (red) participates to the interference process, producing a modified pattern in the photoelectron spectrum (blue curve, right panel). In all panels Ω indicates the photon energy while ε the electron kinetic energy.

[Figs. 2(e)-(f), see Supplementary Sec. S2.5]. The temporal profiles used in these calculations match those in Fig. 1(a), with no delay between the pulses. For TL

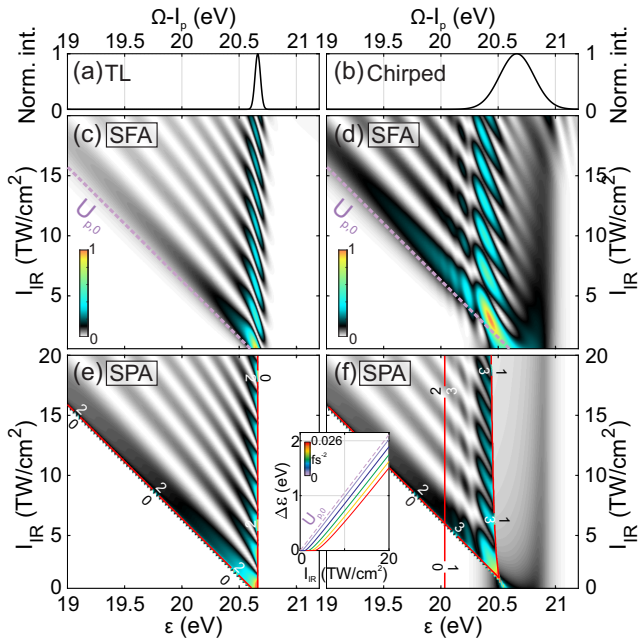

FIG. 2. Spectrum of an XUV pulse corresponding to a FWHM time duration of about 33 fs: **(a)**, TL, **(b)** chirped ($c_\Omega = 8.1 \times 10^{-3}\,\mathrm{fs}^{-2}$). The ionization potential of Ne ($I_p = 21.5646\,\mathrm{eV}$) has been subtracted to the photon energy Ω for a direct comparison with the other panels presenting the electron kinetic energy ε. Photoelectron spectra of Ne calculated with the SFA while changing the IR peak intensity I_{IR} [same temporal profile as in Fig. 1(a)], for the TL, **(c)**, and chirped, **(d)**, XUV pulse. **(e)**, **(f)**, Same quantity calculated within the SPA. The red contour lines mark the regions with a diverse number of stationary solutions, indicated by the nearby numbers. Only solutions for which $E_{\Omega,0}(t_i) \geq 10^{-4}$, are considered. Inset: width of the energy region with stationary solutions, $\Delta\varepsilon$, as a function of I_{IR} and c_Ω.

XUV pulses (left column), LADI produces fringes that increase in number and shift towards lower electron energies with increasing IR intensity, following $U_{p,0}$ [dashed violet curve in Fig. 2(c)]. This pattern can be reproduced by SPA, showing that it originates from the interference of only two quantum trajectories [Fig. 2(e)]. Chirped XUV pulses lead to a modified spectral map [Fig. 2(d)] that can still be explained within the SPA [Fig. 2(f)]. While the exact shape of the interference pattern depends on the used laser parameters [see Supplementary Secs. S2.4, S2.5], the width of the energy region with stationary solutions can be evaluated by computing $\Delta\varepsilon = \varepsilon(t_M) - \varepsilon(t_m)$, where $t_{M,m}$ are the times corresponding to the local maximum and minimum of $\varepsilon(t)$ [see Fig. 1(e) and Supplementary Sec. S2.6]. For a given XUV spectrum, $\Delta\varepsilon$ scales mostly linear with IR intensity and increases with decreasing c_Ω [inset of Fig. 2(f)], suggesting that a smaller chirp will allow for the observation of cLADI on a broader energy range. Nevertheless, the smaller the chirp the shorter the XUV pulse, ultimately leading to no cLADI if the pulse duration becomes shorter than the IR one. Thus, optimizing this effect requires balancing the XUV duration and the extent of $\Delta\varepsilon$.

Within $\Delta\varepsilon$ three stationary solutions exist for each final electron energy. Two correspond to the standard LADI solutions which temporally lay within the IR envelope [orange and green in Fig. 1(e)], while the chirp solution [red in Fig. 1(e)] exists when $U_p(t_i) \simeq 0$. Following Eq. (2), the related ionization times are given by:

$$t_c \simeq -\frac{\Omega_0 - \varepsilon - I_p}{2c_\Omega}, \tag{3}$$

and increase linearly with the electron energy ε [black-dotted lines in Fig. 1(e)]. If $|t_c|$ is large compared to the XUV duration, its contribution to the photoelectron spectrum becomes negligible (see Supplementary Sec. S2.5) and only the two standard families of stationary solutions contribute to the photoelectron spectrum [upper-left corner in Fig. 2(f)]. This explains why cLADI and LADI produce qualitatively similar spectral maps at high IR intensities and low electron energies. However, near Ω_0 [where three solutions exist in Fig. 2(f)], the contribution of t_c becomes significant, introducing a finer fringe pattern that does not scale with $U_{p,0}$. This new interference pattern extends at high energies into the pulse spectrum, where only one real stationary solution exists, offering a unique opportunity to study quantum transitions between different numbers of "trajectories" (stationary solutions) and a novel platform for applications of catastrophe optics [36]. Moreover, since Eq. (3) shows that t_c does not depend on the IR parameters, cLADI may enable holographic reconstruction techniques. Indeed, while only the phase difference between the interfering stationary points is encoded in the LADI spectrum, if the XUV parameters have been properly characterized, t_c and $\phi(t_c)$ can be computed, allowing for the extraction of the absolute phases $\phi(t_1)$ and $\phi(t_2)$, and enabling the reconstruction of the electronic wavepacket from the measured interference pattern.

To demonstrate the feasibility of cLADI, we performed two-color photoemission experiments at the ELI ALPS HR Condensed beamline [37]. The setup employed 15-fs IR pulses centered at 1030 nm to generate XUV radiation via high-harmonic generation (HHG) at a 100-kHz repetition rate. A time-delay-compensated monochromator (TDCM) selected the 35$^{\text{th}}$ harmonic at about 42.2 eV [38, 39]. While the femtosecond chirp of the harmonic radiation can be controlled by adjusting the driving laser properties [40, 41], in a TDCM it can also be tuned by introducing an imbalance between the two stages [42, 43]. A portion of the IR beam, with

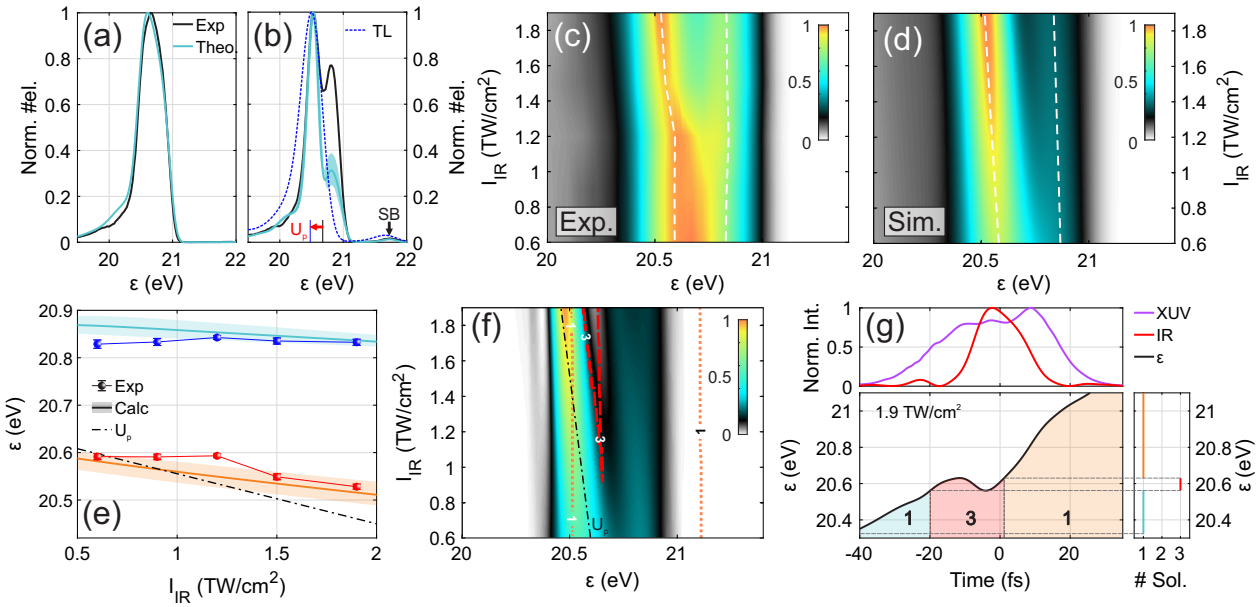

FIG. 3. Experimental (black) and calculated (light blue) photoelectron spectrum for crossed XUV and IR polarizations, with $I_{IR} = 0$ **(a)**, and 1.9 TW/cm^2, **(b)**. The shaded light-blue area in (b) shows the deviation of the calculated spectra in a delay range of ± 3 fs between the two pulses. The dotted-blue curve represent the photoelectron spectrum obtained with a TL XUV pulse of identical spectral bandwidth. **(c)**, **(d)**, Experimental and calculated Ne spectra as a function of the IR intensity, I_{IR}, and electron kinetic energy ε. **(e)**, Energy position of the local maxima in the photoelectron spectra as extracted form the measurements (full dots) and from the calculations (full curves and shaded areas). **(f)**, Photoelectron spectra calculated only along the XUV polarization axis and for ideal detection. The red dashed and orange dotted lines indicate the regions with 3 or 1 stationary solutions. The black dash-dotted curve marks $U_{p,0}$. **(g)**, Top panel, XUV and IR intensity envelopes retrieved with STRIPE and used in the calculations. Bottom panel, energy shift felt by the electron wavepacket, $\varepsilon(t)$, (left) and number of stationary solutions (right), calculated for $I_{IR} = 1.9$ TW/cm^2.

a controlled delay, was collinearly recombined with the XUV and focused onto a Ne gas target. Photoelectrons were collected using a time-of-flight (TOF) spectrometer aligned with the XUV polarization axis (following the scheme in Ref. [30]). The photoelectron count per shot was optimized to ≈ 1 to enhance the signal-to-noise ratio. Full temporal characterization of the pulses using STRIPE (simplified trace reconstruction in the perturbative regime) [44] confirmed that the XUV pulses were chirped, with $c_\Omega = 8.9 \times 10^{-3}$ fs^{-2} (FWHM duration of 33 fs, TL duration of 5.2 fs), while the IR pulses remained nearly TL with a 15-fs FWHM [see intensity envelopes in Fig. 3(g)], closely matching the conditions of Fig. 2.

Figure 3(a) presents the experimental (black curve) and theoretical (light-blue curve) photoelectron spectra for Ne ionization without the dressing IR pulse. Simulations based on the SFA model (see Supplementary Sec. S2.1), incorporating the Ne $2p$ spin-orbit splitting and instrumental response function (responsible for the asymmetric low-energy tail), show no evident interference. Introducing an intense (1.9 TW/cm^2) IR pulse at zero delay with crossed polarization significantly alters the spectrum [Fig. 3(b)], shifting the main peak and splitting it into two maxima. This splitting vanishes in simulations using TL XUV pulses (blue dotted curve), indicating its origin in cLADI. A secondary peak at 21.75 eV corresponds to the creation of a sideband (SB) arising from the MP term $\mathbf{p} \cdot \mathbf{A}_\omega$, which affects those electrons that are not emitted perpendicularly to the IR field but fall within the finite collection angle of the spectrometer (about 14° of total angle). This effect is reproduced in simulations incorporating the Ne photoionization cross-section and angular distribution [45] (see Supplementary Sec. S2.1). For the chirped pulses, the light-blue shaded area displays the deviation of the calculated spectra in a delay range of ± 3 fs around $\tau = 0$ fs. The double-peaked structure survives, underlying the robustness of the cLADI pattern against zero delay uncertainty. To further investigate the origin of the main spectral splitting, we recorded the photoelectron kinetic-energy distribution while varying the IR intensity between 0.6 and 1.9 TW/cm^2 [Fig. 3(c), experiment; Fig. 3(d), SFA predictions]. We observed that the local maxima in the photoelectron spectra [white dashed lines in Fig. 3(c), full dots in Fig. 3(e)] shift with IR intensity in a way not simply captured by $U_{p,0}$ [dot-dashed black curve in Fig. 3(e)] but accurately reproduced by SFA calculations [white dashed lines in Fig.3(d), solid curves in Fig. 3(e)]. A sim-

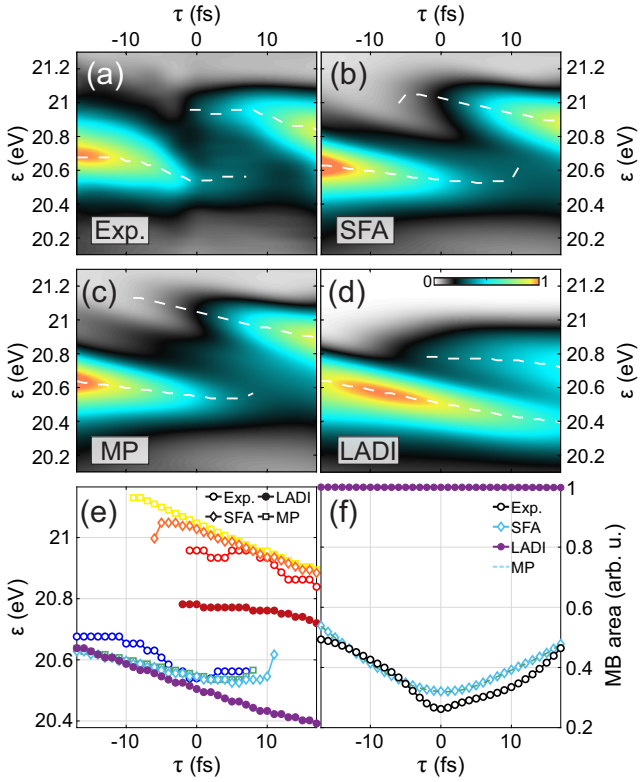

FIG. 4. **(a)**, Portion of the experimental Ne spectrogram obtained with parallel IR and XUV polarizations, showing the electron counts vs. kinetic energy, ε, and delay τ. The IR and XUV pulses used are the same as in Fig. 3, while $I_{IR} = 1.9\,\mathrm{TW/cm^2}$. Spectrograms simulated by using the experimental pulses and the total SFA formula, **(b)**, considering only the MP term, **(c)**, or the cLADI term **(d)**. Comparison of the energy position of the local maxima, **(e)**, and spectral area, **(f)**, extracted from panels (a)-(d). Open circles mark the experimental data while the SFA, MP and LADI calculations are represented with open diamonds, full circles and open squares, respectively.

ilar behavior is found when considering only perfect emission along the XUV polarization axis (i.e. $\mathbf{p} \cdot \mathbf{A}_\omega = 0$), neglecting instrumental response function and spin-orbit splitting [Fig. 3(f)]. Analyzing the number of active stationary points in this case (contour lines) further confirms that the observed spectral splitting originates from three-path interference, i.e., cLADI [Fig. 3(g)]. Notably, in the standard LADI regime, simulations either yield a simple $U_{p,0}$-shift when using TL XUV pulses with the same bandwidth (FWHM $\sim 5\,\mathrm{fs}$) or produce a finer interference pattern when maintaining the 33-fs duration. In the latter case, the experimental instrumental response function limits clear detection.

A vanishing MP term is essential for the observation of LADI and cLADI. To test this, we repeated the experiment at the highest available IR intensity with parallel IR and XUV polarizations. The spectral components associated with direct XUV ionization (main band, MB) as a function of delay τ are shown in Fig. 4(a). Here a positive delay corresponds to the IR pulse arriving earlier. At zero delay, the initial single peak [same as in Fig. 3(a)] splits into two local maxima [white dashed curves in Fig. 4(a)]. This behavior is well reproduced by SFA calculations that include both MP and cLADI contributions [Fig. 4(b)] or consider only the MP term [Fig. 4(c)]. However, pure cLADI [Fig. 4(d), equivalent to crossed IR and XUV polarizations] fails to reproduce the precise position of the local maxima [Fig. 4(e)] and the main-band depletion [Fig. 4(f)]. Thus, our analysis shows that with parallel polarizations, the photoelectron spectrum is dominated by MP-induced sidebands (see Supplementary Sec. S1.5), which obscure the LADI pattern.

Summarizing, we have introduced a new regime of laser-assisted dynamic interference driven by chirped XUV pulses (cLADI), extending the control of photoelectron dynamics beyond conventional approaches. Through theoretical modeling and stationary-phase analysis, we demonstrated that cLADI provides a powerful mean to manipulate the temporal trajectories of photoemitted electronic wavepackets in the continuum. Our analysis reveals that observation of LADI in standard parallel-polarization schemes [25] is complicated by the concurrent interplay of MP phenomena. Conversely, our two-color experiment with crossed polarizations confirms that cLADI remains detectable even at relatively low IR intensities.

Our finding reveals that by precisely tailoring the temporal profiles of XUV and IR fields, it is possible to imprint complex energy-time structures onto electronic wavepackets immediately after photoionization, enabling fine control over photoelectron trajectories. Notably, in cLADI, the number of interfering pathways depends directly on the XUV intensity profile, offering a unique opportunity to explore transitions between ionization regimes characterized by different numbers of stationary solutions. Such transitions are of fundamental interest in strong-field physics, where quasi-classical trajectories are essential to interpret quantum dynamics of high-harmonic generation [46] and above-threshold ionization [47]. Furthermore, the emergence of a new family of stationary solutions, absent in the unchirped case and independent of the IR intensity, suggests that cLADI could be combined with holographic techniques for a complete reconstruction of interfering wavepackets.

While demonstrated here for a quadratic chirp, cLADI can be extended to more complex phase profiles, enabling control over additional interference pathways and expanding the toolbox for ultrafast quantum control. By establishing cLADI as a distinct form of multi-path quantum interference, our results lay the foundation for its application in ultrafast spectroscopy, free from spectral overlap and multiphoton constraints. This work opens

new avenues for the precision control of electron dynamics and enhances our ability to probe and manipulate ultrafast processes in complex systems.

This project has received funding from the European Research Council (ERC) under the European Union's Horizon 2020 research and innovation programme (grant agreement No. 848411 title AuDACE) and from MIUR FARE (Grant No. R209LXZRSL, title PHorTUNA). JMD acknowledges support from the Olle Engkvist Foundation: 194-0734, the Knut and Alice Wallenberg Foundation: 2019.0154, and the Swedish Research Council: 2024-04247. The ELI-ALPS project (GINOP-2.3.6-15-2015-00001) is supported by the European Union and co-financed by the European Regional Development Fund. The work of B.M. was supported by the Janos Bolyai Research Scholarship of the Hungarian Academy of Sciences. PEJ, EA, MP and VP acknowledge the support of the Knut and Alice Wallenberg Foundation (2020.0111), the Swedish Research Council (2021-05992), and the Helmholtz Foundation through the Helmholtz-Lund International Graduate School (HELIOS, HIRS-0018). The authors FF and LP acknowledge the support from the project "IPHOQS: Integrated Infrastructure Initiative in Photonic and Quantum Sciences - Activity 3.1: Optics for ultraintense and ultrashort beams", funded in the framework of the National Recovery and Resilience Plan.

* federico.vismarra@phys.chem.ethz.ch; Present address: Department of Chemistry, Laboratorium für Physikalische Chemie, ETH Zürich, Vladimir-Prelog-Weg 2, Zürich, 8093, Switzerland
† These authors contributed equally to this work
‡ per.eng-johnsson@fysik.lth.se
§ marcus.dahlstrom@matfys.lth.se
¶ matteo.lucchini@polimi.it

[1] F. Krausz and M. Ivanov, Attosecond physics, Reviews of Modern Physics **81**, 163 (2009).
[2] R. Borrego-Varillas, M. Lucchini, and M. Nisoli, Attosecond spectroscopy for the investigation of ultrafast dynamics in atomic, molecular and solid-state physics, Reports on Progress in Physics **85**, 066401 (2022).
[3] Y. Mairesse and F. Quéré, Frequency-resolved optical gating for complete reconstruction of attosecond bursts, Physical Review A **71**, 011401 (2005).
[4] H. Muller, Reconstruction of attosecond harmonic beating by interference of two-photon transitions, Applied Physics B **74**, s17 (2002).
[5] L. Cattaneo, J. Vos, M. Lucchini, L. Gallmann, C. Cirelli, and U. Keller, Comparison of attosecond streaking and RABBITT, Optics Express **24**, 29060 (2016).
[6] J. M. Dahlström, A. L'Huillier, and A. Maquet, Introduction to attosecond delays in photoionization, Journal of Physics B: Atomic, Molecular and Optical Physics **45**, 183001 (2012).
[7] R. Pazourek, S. Nagele, and J. Burgdörfer, Time-resolved photoemission on the attosecond scale: opportunities and challenges, Faraday Discussions **163**, 353 (2013).
[8] H. Laurell, S. Luo, R. Weissenbilder, M. Ammitzböll, S. Ahmed, H. Söderberg, C. L. M. Petersson, V. Poulain, C. Guo, C. Dittel, D. Finkelstein-Shapiro, R. J. Squibb, R. Feifel, M. Gisselbrecht, C. L. Arnold, A. Buchleitner, E. Lindroth, A. F. Kockum, A. L'Huillier, and D. Busto, Measuring the quantum state of photoelectrons, Nature Photonics (2025).
[9] P. V. Demekhin and L. S. Cederbaum, Dynamic Interference of Photoelectrons Produced by High-Frequency Laser Pulses, Phys. Rev. Lett. **108**, 253001 (2012).
[10] M. Baghery, U. Saalmann, and J. M. Rost, Essential Conditions for Dynamic Interference, Phys. Rev. Lett. **118**, 143202 (2017).
[11] W.-C. Jiang and J. Burgdörfer, Dynamic interference as signature of atomic stabilization, Opt. Express **26**, 19921 (2018).
[12] P. H. Bucksbaum, R. R. Freeman, M. Bashkansky, and T. J. McIlrath, Role of the ponderomotive potential in above-threshold ionization, J. Opt. Soc. Am. B **4**, 760 (1987).
[13] N. B. Delone and V. P. Krainov, Ac stark shift of atomic energy levels, Physics-Uspekhi **42**, 669 (1999).
[14] M. Gavrila, Atomic stabilization in superintense laser fields, J. Phys. B: At. Mol. Opt. Phys. **35**, R147 (2002).
[15] A. Tóth, S. Borbély, and A. Csehi, Dynamic interference in below-threshold ionization, Physical Review A **108**, L061101 (2023).
[16] A. D. Müller, E. Kutscher, A. N. Artemyev, L. S. Cederbaum, and P. V. Demekhin, Dynamic interference in the resonance-enhanced multiphoton ionization of hydrogen atoms by short and intense laser pulses, Chemical Physics **509**, 145 (2018).
[17] A. Tóth and A. Csehi, Probing strong-field two-photon transitions through dynamic interference, Journal of Physics B: Atomic, Molecular and Optical Physics **54**, 035005 (2021).
[18] N. S. Simonović, D. B. Popović, and A. Bunjac, Manifestations of rabi dynamics in the photoelectron energy spectra at resonant two-photon ionization of atom by intense short laser pulses, Atoms **11**, 20 (2023).
[19] A. A. Elarabi and A. Csehi, Transition from rabi oscillations to dynamic interference: The multipeak pattern of the autler-townes doublet revisited, Physical Review A **111**, 033107 (2025).
[20] S. Nandi, E. Olofsson, M. Bertolino, S. Carlström, F. Zapata, D. Busto, C. Callegari, M. D. Fraia, P. Eng-Johnsson, R. Feifel, G. Gallician, M. Gisselbrecht, S. Maclot, L. Neoričić, J. Peschel, O. Plekan, K. C. Prince, R. J. Squibb, S. Zhong, P. V. Demekhin, M. Meyer, C. Miron, L. Badano, M. B. Danailov, L. Giannessi, M. Manfredda, F. Sottocorona, M. Zangrando, and J. M. Dahlström, Observation of rabi dynamics with a short-wavelength free-electron laser, Nature **608**, 488 (2022).
[21] X. Zhang, Y. Zhou, Y. Liao, Y. Chen, J. Liang, Q. Ke, M. Li, A. Csehi, and P. Lu, Effect of nonresonant states in near-resonant two-photon ionization of hydrogen, Physical Review A **106**, 063114 (2022).
[22] E. Olofsson and J. M. Dahlström, Photoelectron signature of dressed-atom stabilization in an intense xuv field, Physical Review Research **5**, 043017 (2023).
[23] D. Rogus and M. Lewenstein, Resonant ionisation by smooth laser pulses, Journal of Physics B: Atomic and Molecular Physics **19**, 3051 (1986).

[24] M. Bertolino, S. Carlström, J. Peschel, F. Zapata, E. Lindroth, and J. M. Dahlström, Thomas-Reiche-Kuhn correction for truncated configuration-interaction spaces: Case of laser-assisted dynamical interference, Physical Review A **106**, 043108 (2022).

[25] M. Li, M.-F. Xie, H. Wang, L. Jia, J. Li, W. Wang, J. Cai, X. Hong, X. Shi, Y. Lv, X. Zhao, S. Luo, W.-C. Jiang, L.-Y. Peng, and D. Ding, Observation of laser-assisted dynamic interference by attosecond controlled photoelectron spectroscopy, Physical Review Letters **133**, 253201 (2024).

[26] M. Lewenstein, P. Balcou, M. Y. Ivanov, A. L'Huillier, and P. B. Corkum, Theory of high-harmonic generation by low-frequency laser fields, Physical Review A **49**, 2117 (1994).

[27] M. Y. Ivanov, M. Spanner, and O. Smirnova, Anatomy of strong field ionization, Journal of Modern Optics **52**, 165 (2005).

[28] K. Amini, J. Biegert, F. Calegari, A. Chacón, M. F. Ciappina, A. Dauphin, D. K. Efimov, C. F. de Morisson Faria, K. Giergiel, P. Gniewek, A. S. Landsman, M. Lesiuk, M. Mandrysz, A. S. Maxwell, R. Moszyński, L. Ortmann, J. A. Pérez-Hernández, A. Picón, E. Pisanty, J. Prauzner-Bechcicki, K. Sacha, N. Suárez, A. Zaïr, J. Zakrzewski, and M. Lewenstein, Symphony on strong field approximation, Reports on Progress in Physics **82**, 116001 (2019).

[29] M. Kitzler, N. Milosevic, A. Scrinzi, F. Krausz, and T. Brabec, Quantum Theory of Attosecond XUV Pulse Measurement by Laser Dressed Photoionization, Physical Review Letters **88**, 173904 (2002).

[30] M. Lucchini, F. Medeghini, Y. Wu, F. Vismarra, R. Borrego-Varillas, A. Crego, F. Frassetto, L. Poletto, S. A. Sato, H. Hübener, U. D. Giovannini, Ángel Rubio, and M. Nisoli, Controlling floquet states on ultrashort time scales, Nature Communications **13**, 7103 (2022).

[31] M. Lucchini, Floquet interpretation of attosecond rabbitt traces, Physical Review A **108**, 013117 (2023).

[32] A. Nayak, M. Dumergue, S. Kühn, S. Mondal, T. Csizmadia, N. Harshitha, M. Füle, M. Upadhyay Kahaly, B. Farkas, B. Major, V. Szaszkó-Bogár, P. Földi, S. Majorosi, N. Tsatrafyllis, E. Skantzakis, L. Neoričić, M. Shirozhan, G. Vampa, K. Varjú, P. Tzallas, G. Sansone, D. Charalambidis, and S. Kahaly, Saddle point approaches in strong field physics and generation of attosecond pulses, Physics Reports **833**, 1 (2019).

[33] D. G. Arbó, K. L. Ishikawa, K. Schiessl, E. Persson, and J. Burgdörfer, Intracycle and intercycle interferences in above-threshold ionization: The time grating, Physical Review A **81**, 021403 (2010).

[34] A. A. Gramajo, R. D. Picca, C. R. Garibotti, and D. G. Arbó, Intra- and intercycle interference of electron emissions in laser-assisted xuv atomic ionization, Physical Review A **94**, 053404 (2016).

[35] R. D. Picca, M. F. Ciappina, M. Lewenstein, and D. G. Arbó, Laser-assisted photoionization: Streaking, sideband, and pulse-train cases, Physical Review A **102**, 043106 (2020).

[36] M. V. Berry and C. Upstill, IV Catastrophe Optics: Morphologies of Caustics and Their Diffraction Patterns, in *Progress in Optics*, Vol. 18, edited by E. Wolf (Elsevier, 1980) pp. 257–346.

[37] P. Ye, T. Csizmadia, L. G. Oldal, H. N. Gopalakrishna, M. Füle, Z. Filus, B. Nagyillés, Z. Divéki, T. Grósz, M. Dumergue, P. Jójárt, I. Seres, Z. Bengery, V. Zuba, Z. Várallyay, B. Major, F. Frassetto, M. Devetta, G. D. Lucarelli, M. Lucchini, B. Moio, S. Stagira, C. Vozzi, L. Poletto, M. Nisoli, D. Charalambidis, S. Kahaly, A. Zaïr, and K. Varjú, Attosecond pulse generation at elialps 100 khz repetition rate beamline, Journal of Physics B: Atomic, Molecular and Optical Physics **53**, 154004 (2020).

[38] L. Poletto, P. Villoresi, F. Frassetto, F. Calegari, F. Ferrari, M. Lucchini, G. Sansone, and M. Nisoli, Time-delay compensated monochromator for the spectral selection of extreme-ultraviolet high-order laser harmonics, Review of Scientific Instruments **80**, 123109 (2009).

[39] T. Csizmadia, Z. Filus, T. Grósz, P. Ye, L. Gulyás Oldal, M. De Marco, P. Jójárt, I. Seres, Z. Bengery, B. Gilicze, M. Lucchini, M. Nisoli, F. Frassetto, F. Samparisi, L. Poletto, K. Varjú, S. Kahaly, and B. Major, Spectrally tunable ultrashort monochromatized extreme ultraviolet pulses at 100 kHz, APL Photonics **8**, 056105 (2023).

[40] H. T. Kim, I. J. Kim, K.-H. Hong, D. G. Lee, J.-H. Kim, and C. H. Nam, Chirp analysis of high-order harmonics from atoms driven by intense femtosecond laser pulses, Journal of Physics B: Atomic, Molecular and Optical Physics **37**, 1141 (2004).

[41] K. Varjú, Y. Mairesse, B. Carré, M. B. Gaarde, P. Johnsson, S. Kazamias, R. López-Martens, J. Mauritsson, K. J. Schafer, P. Balcou, A. L'huillier, and P. Salières, Frequency chirp of harmonic and attosecond pulses, Journal of Modern Optics **52**, 379 (2005).

[42] F. Frassetto, P. Villoresi, and L. Poletto, Optical concept of a compressor for xuv pulses in the attosecond domain, Optics Express **16**, 6652 (2008).

[43] M. Mero, F. Frassetto, P. Villoresi, L. Poletto, and K. Varjú, Compression methods for xuv attosecond pulses, Optics Express **19**, 23420 (2011).

[44] G. L. Dolso, G. Inzani, N. Di Palo, B. Moio, F. Medeghini, R. Borrego-Varillas, M. Nisoli, and M. Lucchini, Versatile and robust reconstruction of extreme-ultraviolet pulses down to the attosecond regime, APL Photonics **8**, 076101 (2023).

[45] K. Codling, R. G. Houlgate, J. B. West, and P. R. Woodruff, Angular distribution and photoionization measurements on the 2p and 2s electrons in neon, Journal of Physics B: Atomic and Molecular Physics **9**, L83 (1976).

[46] O. Raz, O. Pedatzur, B. D. Bruner, and N. Dudovich, Spectral caustics in attosecond science, Nature Photon **6**, 170 (2012).

[47] S. A. Kelvich, W. Becker, and S. P. Goreslavski, Caustics and catastrophes in above-threshold ionization, Phys. Rev. A **96**, 023427 (2017).